Article

Study on Deposition Conditions in Coupled Polysilicon CVD Furnaces by Simulations

Shengtao Zhang [1], Hao Fu [1], Guofeng Fan [2], Tie Li [3], Jindou Han [1] and Lili Zhao [1,*]

1   School of Chemistry and Chemical Engineering, Harbin Institute of Technology, Harbin 150001, China
2   Soft-Impact China (Harbin), Ltd., Harbin 150028, China
3   Harbin KY Semiconductor, Inc., Harbin 150028, China
*   Correspondence: zhaolili@hit.edu.cn; Tel.: +86-188-4613-0714; Fax: +0451-840-10483

Abstract: Electronic-grade polysilicon is the cornerstone of the information industry. Considering the demand for this material in the semiconductor industry, any technological improvement has great potential benefits. Due to the quality requirements of electronic polysilicon, its preparation process is characterized by low raw material utilization and high cost. Simply increasing the deposition rate by increasing the chemical reaction rate will easily lead to a reduction in the proportion of dense materials. For the first time, a coupled furnace scheme is proposed to improve the utilization of raw materials while maintaining the same deposition quality. The deposition conditions on the surface of silicon rods with different base plate designs were modeled and analyzed using the software PolySim, and a design characterized by a high flow rate and the use of 9 mm and 15 mm nozzles was selected for the coupling scheme. In coupling mode, the simulation results show that the utilization of raw materials is increased by 17.5%, and the deposition rate is increased by 44.9%, while the deposition quality and uniformity remain approximately unchanged. The results show that the coupling scheme with high feed flow is beneficial for significantly improving the deposition conditions and the utilization rate of raw materials, which also provides guidance for material preparation processes with similar principles.

Keywords: electronic polysilicon; flow field; temperature field; boundary layer; coupled furnaces

1. Introduction

With the development of the electronic information industry, semiconductor devices, integrated circuits and other high-tech fields have an increasing demand for electronic-grade (EG) high-purity polysilicon [1–3]. The modified Siemens process is the mainstream process for the production of high-purity polysilicon [4], accounting for more than 78% of the global production capacity [5]. The reduction process is the core process of the modified Siemens method. The principle of this method is that raw material with high purity, including trichlorosilane (TCS) and hydrogen (H_2), enter the reactor through nozzles in the base plate, and a chemical vapor deposition reaction (CVD) occurs on the surface of polysilicon rods at a high temperature around 1323 K [6,7]. As a result, the diameters of the rods increase with the growth process. Compared with dozens of solar-grade (SG) polysilicon manufacturing enterprises, the number of electronic-grade polysilicon enterprises is very small, and the production is limited [8,9]. Electronic polysilicon has a very high requirement for product purity [10]. SG polysilicon has a minimum of 6 N or 99.9999% purity, while EG polysilicon has 9 N. The atomic fractions of acceptor impurities and donor impurities are usually below 50 ppt and 150 ppt, respectively, which puts forward a very high demand for the impurity control of the whole closed-loop process [11], resulting in extremely high costs.

Energy and material consumption in the reduction stage accounts for a remarkable proportion of the whole production process [12]. Some researchers have tried to decrease production costs from different directions. Luo [13] pointed out that the well-polished

substrate surface suggests an excellent radiation energy-saving capacity. Nie [14] used ceramic lining on a reactor vessel to emit thermal radiation and obtain smoother radial-dependent temperature and thermal stress distributions. However, both of them increase the furnace cost for expensive materials or processing. Sun [15] studied the influence of the reaction temperature on the yield of silicon and power consumption under certain conditions for the production of electronic-grade polysilicon, which showed that higher temperatures are good for unit consumption but need to be as uniform as possible. Some researchers have studied deposition conditions from the perspective of electricity. Nie [16] presented an electrical heating model using alternating current (AC) for the silicon rods. The influences of the location of the silicon rods, AC frequency, the radius of the rod and wall emissivity on the temperature profile and current density were studied through the application of the developed model. Du [17] found that high-frequency current is conducive to reducing the temperature gradient and put forward the concept of the mixed-frequency heating process. The deposition conditions on the surface of the silicon rod in the reactor determine the polysilicon quality and deposition rate, which is hard to improve and related to many factors, such as the uniformity of rod surface temperature, gas flow rate, flow velocity along the rods and so on. Meanwhile, complex operating parameters, including the feed gas, electronic current, reactor shape and the layout of polysilicon rods, nozzles and outlet, can significantly influence the deposition conditions [18]. Since this stage is in a closed environment and the polysilicon rod surface has a very high temperature of around 1323 K during the deposition process [10,19], gas flow in the reactor and the temperature field distribution of the silicon rod surface are difficult to directly and precisely measure and characterize [20]. The PolySim software employed in this study was used as a numerical simulation tool to understand what happens inside the CVD reactor.

In order to improve the utilization rate of raw materials and reduce costs, a coupled furnace scheme is proposed, which means connecting several furnaces in series to change the amounts of raw materials or the flow rate. This concept is expected to achieve exhaust gas recovery, improve the overall conversion rate of raw materials and reduce material and energy consumption. Due to the reduction in raw materials from the first furnace to the next furnace, the feed material quantity needs to be changed to meet requirements for consistent deposition conditions. Usually, the gas inlet nozzles are fixed on the base plate, whose distribution directly determines the injection rate and flow rate of the raw materials supplied. Therefore, it is necessary to carry out simulation studies on furnaces with different characteristics of inlet gases. In this study, the original scheme, a high inlet gas flow velocity scheme and a high inlet gas flow rate scheme were studied and compared. By analyzing the deposition conditions on the surface of the silicon rods, the high flow rate base plate design was selected for the coupling equipment. The deposition characteristics and process parameter results of the coupling equipment were also simulated, which showed good prospects for the coupled reduction furnace scheme.

2. Modeling Process

The CVD furnace used for modeling is a bell jar type, and its main structure is shown in Figure 1a [21]. Numbers 1 to 13 indicate the base plate, electrodes, exhaust gas outlet pipes, mixed gas inlets, mixed gas inlet pipes, base plate coolant inlet pipes, base plate coolant outlet pipes, furnace coolant inlet pipes and outlet pipes, furnace, silicon rods, coolant interlayer and observation window. The 3D model was built and meshed using PolySim software, and the physical meaning of some parameters is shown in Figure 1b. After neglecting the irrelevant details, the key structures of the reactor, such as the inner wall, base plate, gas inlets, gas outlets and polysilicon rods, were abstracted, and the numerical domain required for the modeling of a CVD reactor was obtained. The main geometric parameters of the reactor are shown in Table 1. Due to the need for resistance heating, in actual production, the tops of the two silicon rods will be connected in series through a small segment of the silicon rods in the initial stage. However, in the model, it is simplified into a small segment with an arc shape (bridge part). In order to facilitate

the comparison of the physical field distribution inside the furnace chamber, a silicon rod diameter of 50 mm was preferentially set during 3D modeling.
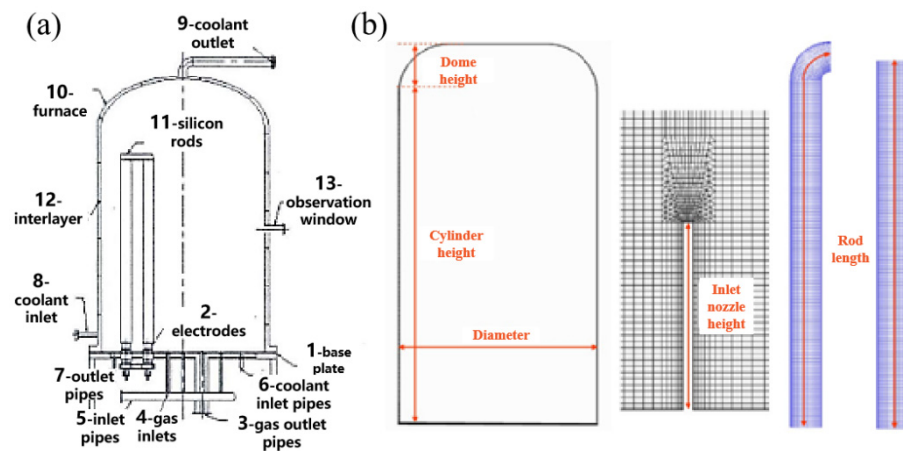

Figure 1. Schematic diagram of bell-type polysilicon reduction furnace: (**a**) Profile; (**b**) Furnace shell and silicon rod.

**Table 1.** Geometrical dimensions of the model of 18-rod CVD reactor.

Categories	Parameters (mm)
Reactor height	2500
Chamber height	320
Reactor diameter	1400
Outlet diameter	35
Silicon rod height	2300
Typical silicon rod diameter	50

The reactor chamber was discretized by a mesh with different kinds of elements (hexahedral, polyhedral and prismatic) to adapt to different characteristics of different domains. To be specific, the prismatic element is used along the polysilicon rods, which allows the extrusion of cells along the cylinders. The boundary layer uses hexahedral structure meshes to provide cell size control, and the polyhedral element is used to discretize the dome due to its complex shape. The first unit of the furnace body boundary layer and the first unit of the silicon rod boundary layer are respectively set to 2 mm and 5 mm, and the transition factor is 1.4. A schematic diagram of the furnace body and silicon rods after meshing is shown in Figure 2. Due to similar settings of mesh generation, the different models have similar grids, which contain about 7 million cells, 19 million faces and 6 million nodes. The minimum orthogonal quality and the maximum aspect ratio are about 0.32 and 32, respectively, and the quality parameters of the grid meet the requirements.
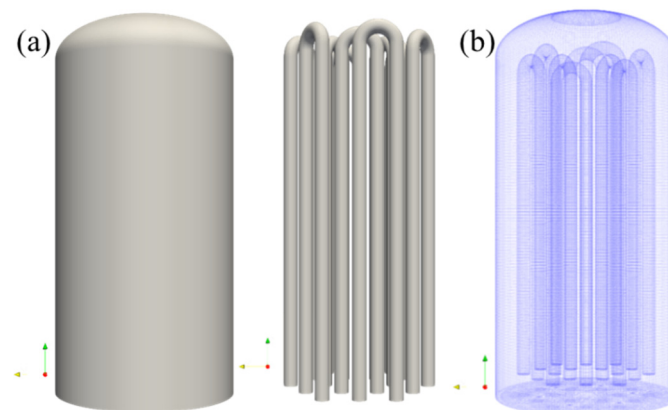
Figure 2. Schematic diagram of furnace body and silicon rods: (**a**) 3D models; (**b**) grid structure.

To explore the requirements of the coupling scheme for the reduction furnace, it is necessary to conduct modeling comparisons from the perspective of increasing the flow rate and increasing the flow rate. In view of this, different base plates with different distributions of gas inlet nozzles were designed, while the overall shape of the equipment was not changed. As shown in Figure 3, the base plate has four rings, including outlet nozzles, silicon rods, inlet nozzles and inner silicon rods from the circumference to the center. Six inlet nozzles are evenly distributed on the nozzle ring, while different schemes have different inlet nozzle arrangements. In design A (original scheme), the inlet nozzles have two diameters of 7 mm and 11 mm, and these nozzles with two diameters are arranged at intervals. In design B (high flow rate scheme), the nozzle diameters are 4.2 mm and 7 mm. Considering the total cross-sectional area of each nozzle, the feed flow rate of scheme B remains unchanged, but the feed flow velocity is increased by 2.5 times. In design C (large flow scheme), the nozzle diameters are 9 mm and 15 mm. The feed flow rate increases twofold. It should be pointed out that the above calculation is simplified, which assumes that the outlet pressure of each nozzle is the same.
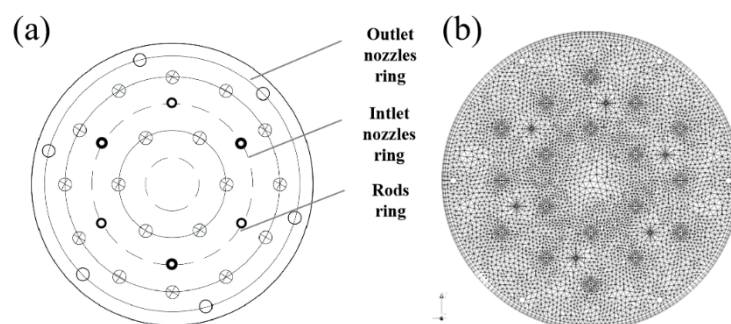
Figure 3. Diagram of base plate: (**a**) structure; (**b**) after meshing.

During the deposition process, large amounts of raw components for the reaction and enough electricity for heating are necessary. For controlling variables, the main process parameters and boundary conditions for modeling these designs are the same, such as electric current, the temperature of the wall, operating pressure, H_2/Si mole ratio and so on, as shown in Table 2. In particular, in order to be close to the actual gas composition, there is some DCS (Dichlorosilane) in the raw material supply. The reduction furnace body is a double-layer structure, and the coolant in the middle layer absorbs the heat of the furnace wall and reduces its temperature. The furnace body is generally made of stainless steel, though some manufacturers use silver-plated materials. The boundary conditions are shown in Table 3. The furnace side wall and base plate are made of the same material in this study.

Table 2. Process parameters.

Schemes	Electric Current (A)	Temperature of Wall (K)	Temperature of Feed Gas (K)	Operating Pressure (kPa)	TCS Flow kg/h	DCS/TCS %	H_2/Si
Design A	1480	370	393	600	550	3	3.24
Design B	1480	370	393	600	550	3	3.24
Design C	1480	370	393	600	1375	3	3.24

Table 3. Boundary conditions.

Categories		Parameters
Emissivity	Silicon rods	0.76
	Furnace wall	0.36
	Base plate	0.36
Heat Conductivity (W/(m·K))	Furnace wall	17
	Base plate	17

During the simulation, processes including turbulent flow (by k-eps model), heat transfer in the gas and inside the rods, radiation and electric current inside rods were modeled. Navier–Stokes equations were solved, together with equations for enthalpy and equations for k and epsilon, respectively. In addition, a surface-to-surface radiation model was used, also known as the view factor model. PolySim 3D was used to solve all of the above equations. The representative process time was selected when the silicon rod diameter was 50 mm so as to evaluate the growth conditions to the greatest extent. To achieve convergence, about 60,000 iterations are required. Residuals for solving equations are less than 0.0001. The heat and radiation imbalances are less than 1.5%, and the mass imbalances are less than 0.5%, which shows that the modeling results converge well. An internal visualizer of PolySim 3D was used to visualize 3D distributions of physical fields, including the temperature field, flow field and boundary layer in the reactor. The modeling results of design A were analyzed and compared with an experiment [22], and highly consistent results were obtained. In the previous study, under similar process conditions and furnace structure, the error of key parameters between the simulation results and the production results was about 4%. The accuracy meeting the requirements in design A provides reliable support for the simulation of the coupling mode.

3. Results and Discussion
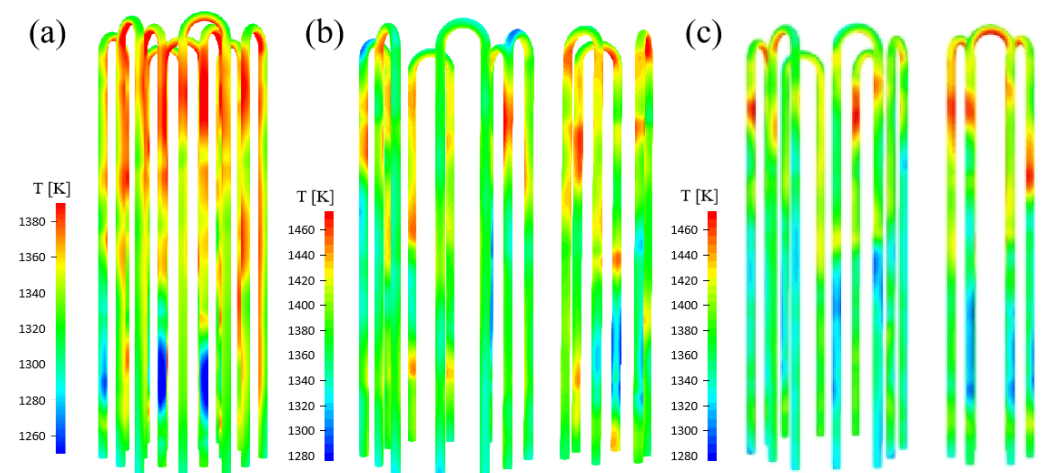
3.1. Temperature Distribution

Although a temperature of around 1300 K is required for polysilicon deposition, the furnace wall maintains a relatively low temperature due to the existence of the interlayer cooling water outside the furnace. Figure 4 shows the temperature distribution inside the furnace with different designs. The temperature of the furnace wall is typically somewhere between 400–460 K, and the mid-upper part has a higher temperature, which corresponds to the higher temperature of silicon rods. In contrast, design C has a lower furnace wall temperature and better distribution uniformity than design B, which is related to the heat consumption of the larger flow of inlet gases. In order to understand the temperature distribution in the furnace cavity, four horizontal sections with different heights (from bottom to top, they are 0.5 m, 1.1 m, 1.7 m and 2.3 m, respectively) and a symmetrical vertical section (passing through two nozzles and the center of the base plate) in the reduction furnace are displayed. Compared with simply increasing the flow velocity, a larger flow rate is conducive to reducing the temperature in the furnace cavity to a certain extent, and its temperature distribution is relatively uniform. The results imply that design C can provide similar uniform deposition conditions to those of the original scheme. Although design B improves the gas inlet flow velocity, the overheated area at the top of the furnace cavity is large and concentrated in the middle and upper parts of the silicon rod, which may lead to an intense gas-phase reaction and the formation of too much silicon dust or powder. In actual production, excessive silicon dust may lead to a short circuit between electrodes or silicon rods, which increases the risk of production process termination and greatly reduces the output.

The heat inside the whole furnace comes from the resistance heating of the silicon rods; the heat is mainly concentrated on the surface of the silicon rod, and the current density in the center of the silicon rod is almost zero [23]. The surface of the silicon rods is where the reaction takes place directly, so the heat transfer state on the surface of the silicon rod deserves attention. The temperature distribution along the rod surface was obtained after the heat transfer was simulated, as shown in Figure 5. The surface temperature of the silicon rods is around 1360–1400 K, but the temperature at the upper part of the silicon rod is particularly high. In the actual process, these areas correspond to areas where a popcorn-shaped structure is most likely to be produced [6]. According to the Arrhenius formula, the reaction rate constant is exponentially related to temperature. The higher surface temperature of the silicon rod greatly increases the reaction deposition rate in this area, resulting in the phenomenon of popcorn-shaped polysilicon near the bridge part of the silicon rods in the actual process, which directly leads to a reduction in the

proportion of dense or qualified materials. The rod surface temperature in design B and design C is generally higher, which means a faster deposition rate and greater preparation efficiency. Meanwhile, the temperature at the silicon rod bridge in designs B and C is not very prominent compared with that in design A, which indicates that the temperature uniformity in design B and design C is improved. The temperature measurement at a height of 2 m for the outer-ring silicon rods shows that the difference between the simulated value and the measured value is equivalent to the error range of the temperature meter, which suggests that the calculated result is reliable.
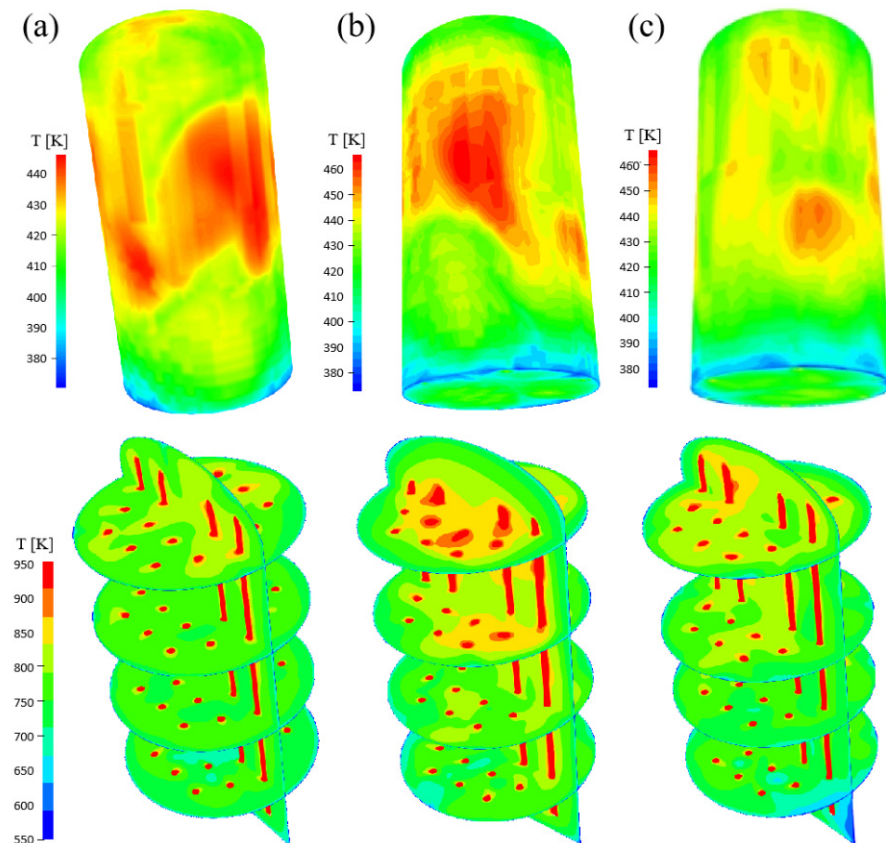
**Figure 4.** Temperature distribution of furnaces. (**a**) Design A; (**b**) design B; (**c**) design C.

Figure 5. Temperature distribution along rod surface. (**a**) Design A; (**b**) design B; (**c**) design C.

A higher temperature in the deposition area will make the surface unstable and produce popcorn polysilicon. The design of the furnace structure means that the silicon rod is easily overheated at the rod bridge part, because more Joule heat is formed at this part due to the concentration of current density. Local overheating of the silicon rod will cause too intense a reaction to form unqualified polysilicon material. In addition, as the feed gas enters from the base plate inlet nozzles, the raw material is gradually heated during its rising process. At the same time, the decrease in the gas flow rate forms a gas stagnation zone, which leads to the failure of the timely replenishment of reaction gas and timely removal of tail mixed gas, and also promotes the heat concentrated in this area. Therefore, in order to improve the utilization rate of raw materials and reduce energy consumption, it is necessary to ensure the uniformity of deposition conditions on the surface of the silicon rods, reduce the overheating area and then improve the reaction rate, especially in the upper part of the reactor. In view of this, the gas flow rate and the thickness of the boundary layer on the surface of the silicon rods in different schemes are analyzed in the following content.

### 3.2. Surface Velocity and Boundary Layer Thickness of Silicon Rods

In order to find ways to relieve the excessively high temperature in the upper bridge area of the silicon rods, the gas flow field in the same section in the three schemes is visualized, as shown in Figure 6. The flow velocity in designs B and C at each cross-section is larger than that of design A, especially at the upper part of the furnace body. The area with a flow velocity above 3.5 m/s increases significantly, while the area with flow velocity below 0.5 m/s decreases significantly, which can be called a gas stagnation zone. Although the gas flow rate decreases rapidly with the rise in the vertical height, the flow velocity of the latter two designs is mostly maintained at 1–1.5 m/s above the height of 1.7 m and even reaches a high flow velocity of 2 m/s at the top-most part. As a result, the gas stagnation zone is greatly reduced, indicating that designs B and C have a relatively stable flow structure on the vertical cross-section. Meanwhile, the flow velocity on the surface of the silicon rod is more noteworthy, since it directly determines the replenishment of reaction gas and the displacement of reaction tail gas. The calculation shows that the average velocity around the silicon rod surface is 1.19 m/s, 1.80 m/s and 2.53 m/s in designs A, B and C, respectively. The increase in flow rate and flow velocity can increase the gas flow velocity on the surface of the silicon rods, which will be more conducive to reducing the volume of the overheated gas area and supplementing the reaction gas in time.
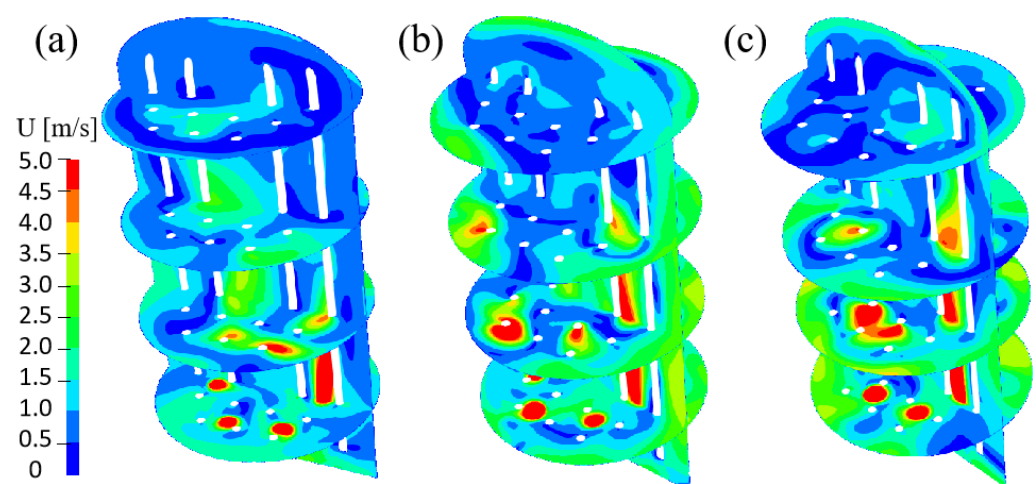
Figure 6. Flow field distribution. (**a**) Design A; (**b**) design B; (**c**) design C (height of horizontal sections is the same as in Figure 4).

The boundary layer thickness in different schemes is plotted to better evaluate the velocity distribution on the surface of the silicon rods, as shown in Figure 7. The boundary layer refers to the thickness of the area with a large velocity gradient near the surface of

the silicon rods. From the wall of the boundary layer, the velocity in this area decreases rapidly along the tangential direction of the wall. Different schemes have similar value distributions, and larger values appear in the upper part and bridge part of the silicon rods. The difference is that the values around the silicon rod bridge part in design A and design B is greater than those in design C, even reaching 7 mm, while the values in design C are mostly between 2–5 mm. In the middle position of the outer-ring silicon rods, designs B and C have smaller values than design A, which means that the boundary layer thickness of design A is larger than that of designs B and C. In order to compare the distribution uniformity, the deviations of the parameter on the surface of the silicon rods at different times in different schemes were obtained and are shown in Table 4. These values also evaluate the uniformity of the boundary layer thickness at different thicknesses of silicon rods (different deposition stages). The boundary layer thickness deviation in design A is the lowest, with an average of 46.6%. Meanwhile, the average values of design B and design C reach 50% and 48%, respectively. These values show that the increasing flow rate and increasing flow velocity achieve smaller boundary layer thickness but also improve the non-uniformity of the boundary layer on the surface of the silicon rods, especially when the diameter of the silicon rod is small. By comparison, design C has better uniformity than design B, and its boundary layer thickness deviation is closer to that of design A, which can provide both better gas flow structure and better polysilicon deposition conditions. Therefore, design C is determined as the base plate scheme for the reduction furnaces in coupled mode.
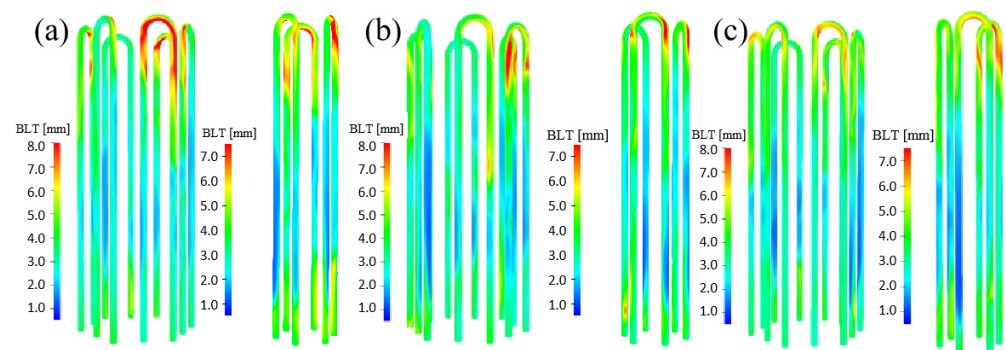
**Figure 7.** Boundary layer thickness along the rods. (**a**) Design A; (**b**) design B; (**c**) design C.

Table 4. Boundary layer thickness deviation (%).

Rod Diameter	Design A	Design B	Design C
50 mm	47.8	53	51.8
90 mm	45.3	48	44.1
125 mm	-	48.9	48.1
Average value	46.6	50.0	48.0

3.3. Results of Coupling Scheme

In coupling mode, several reduction furnaces are connected in series to maximize the utilization of raw materials, which also provides the possibility to make full use of the heat of exhaust gas. Since the conversion rate of raw materials is generally about 10%, the influence of the difference in the contents of gas components on the composition of raw materials is ignored in the calculation, and attention is paid to the inlet gas temperature of furnace #1 and furnace #2. With the help of the calculation platform, the pipe between the coupled reduction furnaces with different silicon rod diameters was modeled. With reference to the actual process, the interlayer cooling water temperature was set to 413 K, and the corresponding silicon rod diameter inside the furnace body was 50 mm. The temperature field distribution in the pipe was obtained and is shown in Figure 8. The tail gas of furnace #1 is discharged from the base plate and transported to the inlet nozzles

of furnace #2 through pipes. The outlet temperature of furnace #1 reaches 780 K. From the base plate outlet, the channel is connected to the annular pipeline via a 1 m vertical pipeline. At this time, the gas temperature reaches 622 K, and the temperature decreases by about 158 K. Before the tail gas enters furnace #2, it needs to be cooled by water cooling through a 4 m long pipe, and the temperature drops to 523 K. After the water-cooled pipe, combined with the actual distance, the outlet temperature can be maintained at around 523 K through the thermal insulation pipeline and then connected to reduction furnace #2.
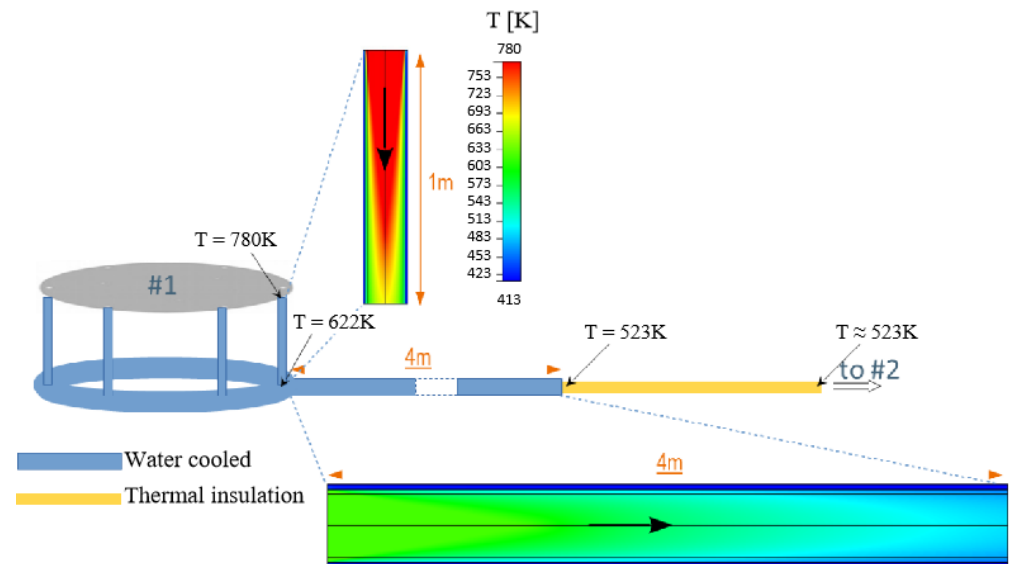
Figure 8. Temperature distribution of tail gas.

The gas temperatures corresponding to the different silicon rod diameters at the outlet of furnace #1 are between 534 K and 745 K, so the inlet temperature of furnace #2 is set according to these values. Further, gas temperature and pipe outlet gas temperature corresponding to different diameters of the silicon rods of coupled reduction furnace #1 and furnace #2, including 30 mm, 50 mm, 90 mm and 125 mm, were calculated, as shown in Table 5. With the increase in diameter, the gas temperature at the outlet gradually increases, and the tail gas temperature gradually rises. However, when the rod diameter reaches more than 90 mm, temperatures remain basically unchanged, and the temperature at the outlet of the pipeline also has similar trends. The pipe outlet temperature of furnace #2 is higher than that of furnace #1, ranging from 170 K to 450 K, which can be easily explained because fresh gas as raw material is heated twice in two furnaces.

Table 5. Temperature of tail gas (K).

Rod Diameter	Tail Gas Temperature	Furnace #1 Pipe Outlet Temperature	Furnace #2 Pipe Outlet Temperature
30 mm	646	472	534
50 mm	780	523	622
90 mm	1025	582	749
125 mm	1028	573	745

In order to calculate the process characteristics of coupling mode, design C was used in both coupled reduction furnaces #1 and #2. The internal physical fields of the two furnaces with different silicon rod diameters were modeled and calculated, and the thickness deviation of the boundary layer is shown in Table 6. The data show that the difference in the thickness deviations of the boundary layer between the two furnaces is very small, which means that the performance of the two reduction furnaces is similar in coupling mode. Design C provides approximate gas flow conditions and ensures the

consistency of the deposition conditions of the two furnaces to a certain extent. At the same time, the boundary layer deviation decreases rapidly and then increases slightly with the increase in the silicon rod diameter. The consistency of deposition conditions is best when the silicon rod diameter is 90 mm, which means that the gas flow structure of design C plays the largest role when silicon rods grow to this diameter. Therefore, the base plate scheme in design C was adopted for the two reduction furnaces, i.e., furnace #1 and furnace #2. The coupling reduction process can adopt single-direction feeding, and the feeding switching step is no longer required.

Table 6. Boundary layer thickness deviation (%).

Rod Diameter	Furnace #1	Furnace #2	Difference
50 mm	51.8	52.3	0.5
90 mm	44.1	45.0	0.9
125 mm	48.1	48.2	0.1

When the diameter of the silicon rods is 90 mm, the flow field and temperature field of the two reduction furnaces are shown in Figure 9. The gas flow rate near the bridge position is still high; an area of more than 2.5 m/s in the 2.3 m height section accounts for more than 50%, and the area of a gas flow rate of less than 0.5 m/s accounts for less than 5%: that is, the gas stagnation area is greatly compressed. Although the temperature in the furnace is high at this growth stage, due to the strong gas flow circulation, the temperature distribution near the silicon rod with the same section in the upper section of the overall reduction furnace is relatively uniform, and the excessive-temperature area in design A no longer exists. Due to the increase in flow velocity and the improvement in flow structure, the surface temperature distribution of the silicon rods is relatively uniform in the upper area of the silicon rods. Only the temperature near the bridge of the silicon rods in the inner ring is slightly higher than 1450 K, and the temperature distribution is mostly concentrated between 1350–1450 K. Compared with furnace #1, the overall gas temperature of furnace #2 is higher for higher inlet temperature. As the diameter of the silicon rod becomes larger, the outer-ring silicon rods have a greater shielding effect on the radiation of the inner silicon rods, and the gas near the inner-ring silicon rods is about 50 K higher than that near the outer-ring silicon rods. In summary, the temperature distribution of the silicon rod is uniform, and the temperature at the bridge is also maintained at an appropriate level, which is conducive to improving the deposition rate and reducing energy consumption while maintaining the uniformity of deposition.

The modeling of the deposition process was also carried out using PolySim software, and the quasi-steady-state method was used to approximate the silicon rod growth process. Based on the former calculated results of different deposition times, including silicon rod surface temperature, boundary layer thickness and its deviation, silicon rod surface flow velocity, inlet gas composition and other parameters, process characteristic parameters such as deposition rate were obtained using the built-in model. While maintaining similar deposition quality between the two reduction furnaces, the expected process characteristics were obtained and are shown in Table 7. The deposition rate in coupling mode reaches 20.8 kg/h, which is 44.9% higher than that of the two single reduction furnaces. The unit energy consumption is 17.2% lower than it was in the original scheme, reaching 74.2 kWh/kg. Although a single furnace in coupling mode has a lower conversion rate of raw materials of about 7%, this parameter increased by 17.5% to 14.1% from 12%. This means that the coupling scheme achieves a significant improvement in the characteristics of the deposition process, significantly reducing the reaction time from about 80 h to 53 h, and the optimization range is obvious.
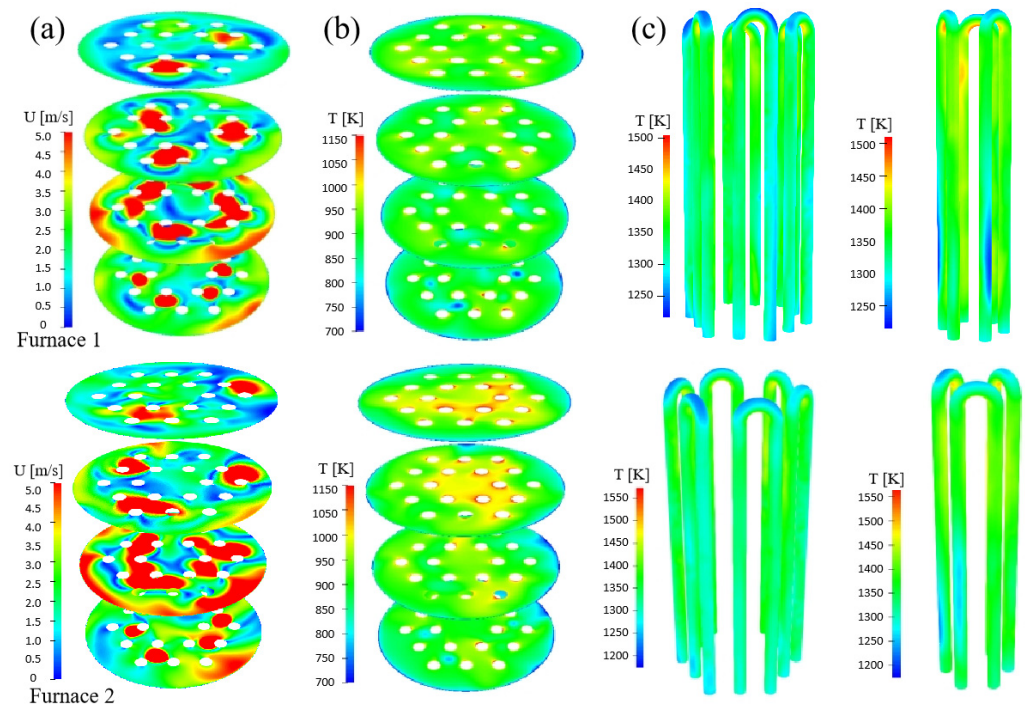
Figure 9. Temperature and velocity distributions. (**a**) Cross-sections of gas velocity; (**b**) cross-sections of temperature; (**c**) rod surface temperature (the height of cross-section is 0.5 m, 1.1 m, 1.7 m and 2.3 m, respectively).

Table 7. Process characteristics.

Parameters	Design A	Furnace #1	Furnace #2	Coupling Mode	Optimization Proportion
Deposition rate (kg/h)	14.08	21.4	19.4	20.4	44.9%
Unit energy consumption (kWh/kg)	89.6	66.6	82.5	74.2	17.2%
Conversion rate (%)	12	7.37	7.22	14.1	17.5%
Process time (h)	79.8	52.6	52.6	52.6	34.1%
Total output (kg)	1124	1124	1020	1072	4.6%

4. Conclusions

For the first time, we propose a coupling device scheme for the preparation of electronic polysilicon by the modified Siemens method and carried out modeling and prediction work on the coupled furnaces based on numerical methods. The distribution of physical fields in the chamber and the uniformity of deposition conditions on the surface of the silicon rods in different base plate designs of the single furnace were analyzed. Based on a large flow rate scheme, the coupled furnaces' silicon rod deposition process was modeled, as well as connecting pipelines and structures. By increasing the flow rate by about 2 times, the coupling mode improves the utilization of raw materials by 17.5% and the deposition rate by 44.9%, while the deposition quality is approximately unchanged. This work provides a new idea for optimizing the deposition characteristics and preparation process of electronic-grade polysilicon at a low cost.

Author Contributions: Conceptualization, S.Z.; methodology, S.Z. and H.F.; software, J.H.; validation, G.F.; formal analysis, H.F. and G.F.; investigation, T.L.; resources, J.H.; data curation, S.Z.; writing—original draft preparation, S.Z.; writing—review and editing, L.Z.; visualization, H.F. and J.H.; supervision, L.Z. and T.L.; project administration, T.L.; funding acquisition, L.Z. All authors have read and agreed to the published version of the manuscript.

Institutional Review Board Statement: Not applicable.

Informed Consent Statement: Not applicable.

Conflicts of Interest: The authors declare no conflict of interest.

References

1.   Ramirez-Marquez, C.; Otero, M.V.; Vazquez-Castillo, J.A.; Martin, M.; Segovia-Hernandez, J.G. Process design and intensification for the production of solar grade silicon. *J. Clean. Prod.* **2018**, *170*, 1579–1593. [CrossRef]
2.   Trinh, A.-K.; González, I.; Fournier, L.; Pelletier, R.; Sandoval, V.J.C.; Lesage, F.J. Solar thermal energy conversion to electrical power. *Appl. Therm. Eng.* **2014**, *70*, 675–686. [CrossRef]
3.   Reznichenko, M. Evolution of Requirements for Solar Grade Silicon. *Procedia Eng.* **2016**, *139*, 41–46. [CrossRef]
4.   Li, X.-G.; Xiao, W.-D. Model on transport phenomena and control of rod growth uniformity in siemens CVD reactor. *Comput. Chem. Eng.* **2018**, *117*, 351–358. [CrossRef]
5.   Bye, G.; Ceccaroli, B. Solar grade silicon: Technology status and industrial trends. *Sol. Energy Mater. Sol. Cells* **2014**, *130*, 634–646. [CrossRef]
6.   del Coso, G.; del Cañizo, C.; Luque, A. Chemical Vapor Deposition Model of Polysilicon in a Trichlorosilane and Hydrogen System. *J. Electrochem. Soc.* **2008**, *155*, 485–491. [CrossRef]
7.   Fang, M.; Xiong, Y.Y.; Yuan, X.Z.; Liu, Y.W. Numerical Analysis of the Chemical Vapor Deposition of Polysilicon in a Trichlorosilane and Hydrogen System. In *International Conference on Applied Energy, Icae2014*; Yan, J., Lee, D.J., Chou, S.K., Desideri, U., Li, H., Eds.; Elsevier Ltd.: Taipei, Taiwan, 2014; pp. 1987–1991.
8.   Wang, Z.; Wei, W. External cost of photovoltaic oriented silicon production: A case in China. *Energy Policy* **2017**, *107*, 437–447. [CrossRef]
9.   Pizzini, S. Towards solar grade silicon: Challenges and benefits for low cost photovoltaics. *Sol. Energy Mater. Sol. Cells* **2010**, *94*, 1528–1533. [CrossRef]
10.   Yadav, S.; Chattopadhyay, K.; Singh, C.V. Solar grade silicon production: A review of kinetic, thermodynamic and fluid dynamics based continuum scale modeling. *Renew. Sustain. Energy Rev.* **2017**, *78*, 1288–1314. [CrossRef]
11.   Nie, Z.; Ramachandran, P.A.; Hou, Y. Optimization of effective parameters on Siemens reactor to achieve potential maximum deposition radius: An energy consumption analysis and numerical simulation. *Int. J. Heat Mass Transf.* **2018**, *117*, 1083–1098. [CrossRef]
12.   Vallerio, M.; Claessens, D.; Logist, F.; Van Impe, J. Multi-Objective and Robust Optimal Control of a CVD Reactor for Polysilicon Production. In *Computer Aided Chemical Engineering*; Klemes, J.J., Varbanov, P.S., Liew, P.Y., Eds.; Elsevier: Amsterdam, The Netherlands, 2014; pp. 571–576.
13.   Luo, X.; Li, S.; Li, G.; Xie, Y.-C.; Zhang, H.; Huang, R.-Z.; Li, C.-J. Cold Spray (CS) Deposition of a Durable Silver Coating with High Infrared Reflectivity for Radiation Energy Saving in the Polysilicon CVD Reactor. *Surf. Coat. Technol.* **2021**, *409*, 126841. [CrossRef]
14.   Nie, Z.; Wang, Y.; Wang, C.; Guo, Q.; Hou, Y.; Ramachandran, P.A.; Xie, G. Mathematical Model and Energy Efficiency Analysis of Siemens Reactor with a Quartz Ceramic Lining. *Appl. Therm. Eng.* **2021**, *199*, 117522. [CrossRef]
15.   Sun, Q.; Chen, H.; Duan, C.; Wan, Y. Effect of Reaction Temperature and Mixture Ratio on Polysilicon Production Process. In *International Conference on Advanced Materials, Processing and Testing Technology*; Trans Tech Publications, Ltd.: Guangzhou, China, 2021.
16.   Nie, Z.; Zhou, Y.; Deng, J.; Wen, S.; Hou, Y. Thermal and Electrical Behavior of Silicon Rod with Varying Radius in a 24-Rod Siemens Reactor Considering Skin Effect and Wall Emissivity. *Int. J. Heat Mass Transf.* **2017**, *111*, 1142–1156. [CrossRef]
17.   Du, P.; Zhou, Y.; Ramachandran, P.A.; Xie, G.; Hou, Y. Numerical Investigations of Heat Transfer and Skin Effect Characteristics within Rods Located in a 48-Rod Siemens Reactor Heated by AC. *Appl. Therm. Eng.* **2021**, *193*, 116972. [CrossRef]
18.   An, L.-S.; Liu, C.-J.; Liu, Y.-W. Optimization of operating parameters in polysilicon chemical vapor deposition reactor with response surface methodology. *J. Cryst. Growth* **2018**, *489*, 11–19. [CrossRef]
19.   Ramos, A.; Rodríguez, A.; del Cañizo, C.; Valdehita, J.; Zamorano, J.C.; Luque, A. Heat losses in a CVD reactor for polysilicon production: Comprehensive model and experimental validation. *J. Cryst. Growth* **2014**, *402*, 138–146. [CrossRef]
20.   Tang, G.; Chen, C.; Cai, Y.; Zong, B.; Cai, Y.; Wang, T. Numerical Simulations of a 96-rod Polysilicon CVD Reactor. *J. Cryst. Growth* **2018**, *489*, 68–71.
21.   Xin, Y.; Shao-fen, W.; Da-zhou, Y. Three-dimensional Numerical Simulation and Optimization of Polysilicon Reduction Furnace Based on Fluent. *Energy Sav. Nonferrous Metall.* **2011**, *27*, 48–52+56.

22. Shimin, L.; Shengtao, Z.; Yinfeng, H.; Min, H. Research on improvement of flow structure of electronic polysilicon reduction furnace based on numerical simulation. *J. Synth. Cryst.* **2019**, *48*, 545–549.
23. Yu, C.; Zhou, Y.M.; Du, P.; Zhao, L.; Zhao, D.; Wang, P.J.; Tian, L.; Xie, G.; Hou, Y.Q. Alternating Current Heating Model of Rods Located in Siemens Reactor. *Fuel Cells* **2021**, *21*, 11–17. [CrossRef]